frontiers in Astronomy and Space Sciences

ORIGINAL RESEARCH
published: 29 October 2021
doi: 10.3389/fspas.2021.710851

Solar Wind Plasma Properties During Ortho-Parker IMF Conditions and Associated Magnetosheath Mirror Instability Response

V. Génot[1]* *and B. Lavraud*[1,2]

[1]Institut de Recherche en Astrophysique et Planétologie, CNRS, Université de Toulouse, CNES, Toulouse, France, [2]Laboratoire d'Astrophysique de Bordeaux, Université Bordeaux, CNRS, Pessac, France

The properties of the solar wind fraction that exhibits an Interplanetary Magnetic Field (IMF) orientation orthogonal to the classical Parker spiral (so-called ortho-Parker) are investigated. We make use of a solar wind plasma categorization scheme, using 10 years of OMNI data, and show that the fractions of the different plasma origins (streamer-belt-origin plasma, coronal-hole-origin plasma, sector-reversal-region plasma and ejecta) identified by this scheme are rather constant when expressed as a function of the IMF orientation whereas the Alfvén Mach number significantly depends on this orientation. This has direct implication on the magnetosheath dynamics and, as an example, the stability of the mirror mode in this compressed plasma is studied thanks to Rankine-Hugoniot anisotropic relations. This study sheds light on previously reported, yet unexplained, observations of a larger occurrence of mirror mode in the magnetosheath downstream of ortho-Parker IMF.

Keywords: heliophysics, plasma physics, space physics, data analysis, solar wind, magnetosheath

OPEN ACCESS

Edited by:
Valeria Mangano,
Institute for Space Astrophysics and Planetology, Italy

Reviewed by:
Jay R. Johnson,
Andrews University, United States
Xiaocheng Guo,
National Space Science Center (CAS), China

***Correspondence:**
V. Génot
vincent.genot@irap.omp.eu

Specialty section:
This article was submitted to Space Physics, a section of the journal Frontiers in Astronomy and Space Sciences

Received: *17 May 2021*
Accepted: *30 August 2021*
Published: *29 October 2021*

Citation:
Génot V and Lavraud B (2021) Solar Wind Plasma Properties During Ortho-Parker IMF Conditions and Associated Magnetosheath Mirror Instability Response. Front. Astron. Space Sci. 8:710851. doi: 10.3389/fspas.2021.710851

1 INTRODUCTION

If the Parker model predicts the orientation of the interplanetary magnetic field (IMF) (Parker, 1963) which commonly adopts the configuration of an Archimedean spiral, observations show that a large fraction of orientations significantly departs from this model, even in the regular solar wind i.e., when solar wind transients such as Coronal Mass Ejections (CME), Co-rotating Interactiob Region (CIR) or magnetic clouds are absent. These so-called ortho-Parker orientations of the IMF, and their origins at the Sun, have attracted attention. For instance Borovsky (2010) proposed the "braiding" concept which explains how small magnetic field deviations (from the Parker direction) close to the Sun are augmented during the solar wind propagation (see also Lockwood et al., 2019 for a related study with the heliocentric distance). These uncommon orientations of the IMF have also singular effects on planetary magnetospheres, and in first instance, their shock, and magnetosheath.

Magnetosheath asymmetry is a long debated subject (Lavraud et al., 2013; Dimmock et al., 2015b; Dimmock et al., 2015a) and the reasons behind it have fueled many studies. The uneven distribution of the IMF orientation, roughly being 75% Parker and 25% ortho-Parker (Génot et al., 2009) when records are taken at ±45° of the main direction, may explain some of the magnetosheath dawn-dusk asymmetries by favouring 1/the occurrence of quasi perpendicular, more laminar shocks on the dusk side and 2/the effects of the foreshock associated turbulence of the dawn side. However, one striking result from studies of the Earth's magnetosheath is the report that ortho-Parker IMF orientations

seem more favorable to trigger the mirror instability (Génot, 2008; Génot et al., 2009; Dimmock et al., 2015b). This instability is ubiquitous in compressed, high β plasma and, in the case of magnetospheres, drives the plasma turbulence during the convection from the shock to the flank by thermalizing the anisotropic shocked solar wind.

In this paper we focus on the orientation of the IMF and show that the associated solar wind plasma has properties that explain how the downstream magnetosheath behaves. In **section 2** we use a long-term (10 years) OMNI data analysis to classify the IMF orientation and we supplement it by the plasma characterization scheme of Xu and Borovsky (2015) to determine where the solar wind plasma originates and what are the properties of each plasma category. In **section 3** we use anisotropic Rankine-Hugoniot relations to infer the magnetosheath properties as a function of the IMF orientation and deduce its stability with respect to the mirror instability. We then address the yet unanswered question about the prevalence of mirror mode occurrence behind the shock for ortho-Parker IMF orientations. All analysis have been done on public data with publicly available software to ensure full reproducibility.

2 INTERPLANETARY MAGNETIC FIELD ORIENTATION AND PLASMA ORIGINS

In the following we use 5 min resolution data from the OMNI dataset (King and Papitashvili, 2005) over the 2008–2018 time range (roughly solar cycle 24) which represents more than one million data records. The IMF orientation is characterized by computing the difference between the theoretical Parker angle Φ_P (depending on the solar wind velocity) and the measured magnetic field angle Φ_B in the ecliptic plane (GSE frame is used):

$$\Phi_P = \arctan_2\left(\frac{-\Omega R}{v_{sw}}\right) \quad (1)$$

$$\Phi_B = \arctan_2\left(B_y/B_x\right) \quad (2)$$

with v_{sw} the solar wind velocity, R is 1AU and $\Omega = 2.7 \times 10^{-7}$ rad/s. The characterization of the IMF orientation by using $\Phi_B - \Phi_P$ has been used by several authors with variations. The first study on the winding of the spiral (Smith and Bieber, 1991) proposed several versions of this characterization and focused on the toward/away orientation of the IMF. Bruno and Bavassano (1997) took into account various values of the co-rotation radius depending on slow/fast winds categories as they analyse Helios 1 and 2 data in the inner heliosphere as close as 0.3 AU. A more complex algorithm combining a solar wind model and near-Earth data and yielding field line mapping between the Sun and the Earth is proposed in Li et al. (2016). For our approach we use the $\arctan_2$ function (or *atan*2 in numerical library) to retrieve angles between ±180°; with this function, in GSE, the Parker orientation at L1 given by **Eq. 1** for v_{sw} =400 km/s is 135°; the classical *atan* function would yield −45° which leads to inconsistency when computing angle differences. The data is then then organized with $|\sin(\Phi_B - \Phi_P)|$ such that Parker orientation corresponds to values close to zero and ortho-Parker orientation to values close to 1 (the directions away/toward are not separated).

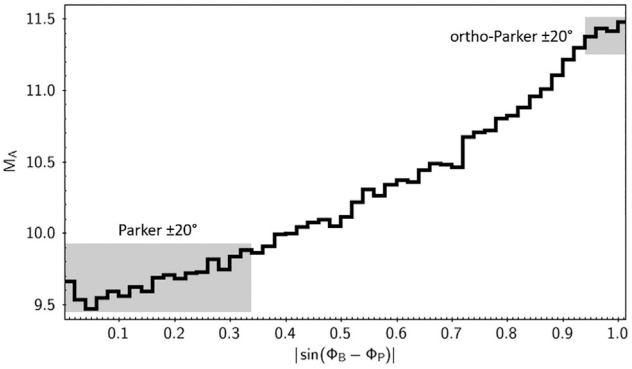

FIGURE 1 | Average of the Mach Alfvén number per bin of $|\sin(\Phi_B - \Phi_P)|$. Parker orientations ± 20° are shown in the grey box on the left and the ortho-Parker orientations ± 20° are shown in the upper right grey box.

Let us now directly investigate the relation between solar wind parameters and the IMF orientation. For all solar wind categories (that will be defined next) the distribution of mean M_A with the field orientation as shown on **Figure 1** presents a distinctive trend: whereas Parker orientations have a mean M_A = 9.7, the ortho-Parker orientations have a larger mean M_A = 11.4. These orientations are taken here in a stricter sense than above by collecting observations oriented around the main orientation within a range ±20° (so defined the Parker dataset represents 32% of the entire collection whereas the ortho-Parker dataset is 9%.) To our knowledge this striking M_A dependence has been overlooked in the literature, perhaps because the causes and the consequences of this behaviour were not clear. While its origin is not explained here, we shall demonstrate one consequence on the magnetosheath in the next section.

To elucidate the causes we track the origin of the solar wind plasma parcels and link them to the IMF orientation. To do so we use the plasma categories as defined in Xu and Borovsky (2015). Following this study the solar wind plasma may be categorized in four types: streamer-belt-origin plasma, coronal-hole-origin plasma, sector-reversal-region plasma, and ejecta, depending on relations between the magnetic field B and plasma moments (proton density n_p, solar wind velocity v_{SW}, and proton temperature T_p). The study by Xu and Borovsky (2015) agregates several published catalogues of events (unperturbed coronal-hole-origin solar wind, pseudostreamer solar wind, the regions around sector reversals, and magnetic clouds) and looks for boundaries in the parameter space constituted of B, n_p, T_p, and v_{SW}. The authors define three parameters:

$$Q_1 = 0.841 B n_p^{-0.315} T_p^{-0.222} v_{SW}^{-0.171} \quad (3)$$

$$Q_2 = 8.77 \times 10^{-11} T_p B^{1.42} v_{SW}^{3.44} n_p^{-2.12} \quad (4)$$

$$Q_3 = 0.0561 T_p B^{0.752} v_{SW}^{0.445} n_p^{-1.14} \quad (5)$$

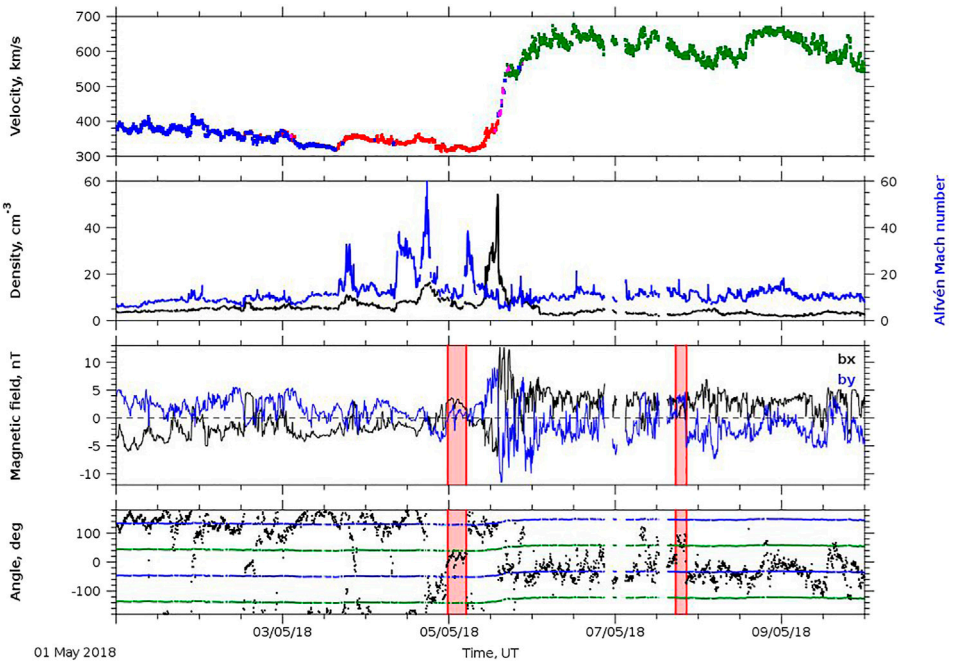

FIGURE 2 | 9 days of solar wind in May 2018 observed at L1. The top panel shows the wind velocity colored by the plasma origins characterized by **Eqs 3**–**5**: SRR (red), SBO (blue), CHO (green), and ejecta (magenta). The second panel shows the density, which peaks at the "ejecta" event seen in magenta on the first panel, and the Alfvén Mach number (in blue) which shows high values for SRR plasmas. The magnetic field components *bx* (black) and *by* (blue) in GSE are plotted on the third panel. The dotted values on the fourth panel is Φ_B (**Eq. 2**, the observed orientation of the magnetic field), the upper blue line corresponds to Φ_P (**Eq. 1**, the common Parker spiral orientation), the bottom blue line to Φ_P-180° (the so-called anti-Parker orientation), the upper green line to Φ_P-90° (ortho-Parker orientation), and the bottom green line to Φ_P-270° (ortho-Parker orientation). Two examples of prolonged intervals (several hours) of ortho-Parker orientations are shaded red in between thick vertical red lines.

from which the plasma origin may be defined: streamer-belt-origin plasma (SBO, for $Q_1 > 1$ and $Q_2 < 1$ and $Q_3 > 1$), coronal-hole-origin plasma (CHO, for $Q_1 < 1$ and $Q_2 > 1$), sector-reversal-region plasma (SRR, for $Q_1 < 1$ and $Q_3 < 1$) and ejecta (for $Q_1 > 1$).

Xu and Borovsky (2015) proposes a very detailed description of the 4 plasma categories including comparisons with already identified/published datasets from which they derive the scheme. It is not our aim to repeat their analysis but let us summarize what are these categories to clarify further discussions. Ejecta are mostly composed of magnetic clouds with low M_A (for instance, 87.5% of Lepping magnetic clouds list fall into that category, as well as 59.5% of solar winds with velocities greater than 850 km/s). Coronal hole origin plasma is composed of high speed streams of coronal origin. Streamer-belt-origin and sector-reversal-region plasmas both come from the streamer belt. The first one is composed of pseudo-streamers, an interval of streamer belt plasma separating two coronal hole regions with the same magnetic polarity. The second ones are related to helmet streamers where a sector reversal (between magnetic polarity) is present. These plasmas are associated with very low velocity and, as noted by Xu and Borovsky (2015), the highest β values are observed for the SRR plasmas and are likely related to the heliospheric plasma sheet. Finally, we note that these characteristics hold at 1 AU and may differ elsewhere in the heliosphere.

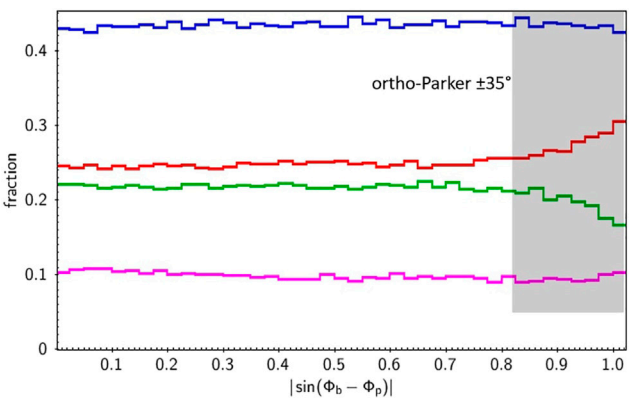

FIGURE 3 | Fractions of the different solar wind populations (SRR in red, SBO in blue, CHO in green, and ejecta in magenta) as a function of $|\sin(\Phi_B - \Phi_P)|$. Parker orientations are to the left and ortho-Parker orientations ± 35° are identified by the grey box to the right.

Figure 2 (first panel) illustrates this characterization scheme with a different colour (on the solar wind velocity time series) for each plasma origin. The plot displays 9 days of data with low velocity (<400 km/s) during the first 5.5 days. The plasma is essentially of streamer belt origin with two successive intervals

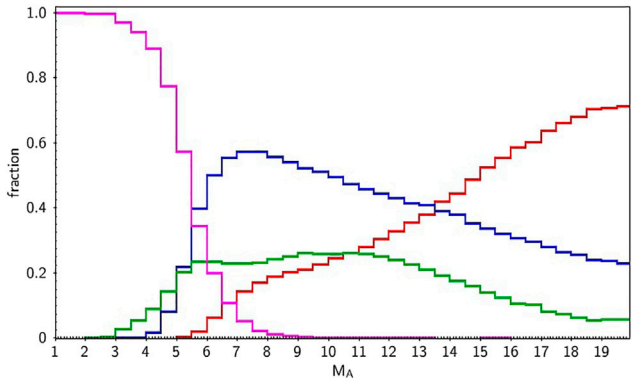

FIGURE 4 | Fractions of the different solar wind populations (SRR in red, SBO in blue, CHO in green and ejecta in magenta) as a function of M_A.

of SBO then SRR plasmas (the later with higher density and Alfvén Mach number than the former). The IMF is mainly Parker-oriented but display a 5 h-long interval of ortho-Parker orientations (first red stripes) and other shorter intervals. Then magnetic cloud plasma is identified for a few hours with an increase of the velocity from 400 to 600 km/s and a magnetic field rotation in the velocity ramp where the density peaks; the plasma is identified as ejecta. This is followed by a high speed wind (600–700 km/s) of low density, identified as of coronal-hole origin, and which displays mostly anti-Parker orientation (angle ~−45°) sometimes alternating with ortho-Parker orientation field (one 3 h-interval is highlighted in red between the second set of thick red lines). As a note for further exploration, we note here that the typical duration of non-Parker events at 1 AU, as defined and analyzed in Lockwood et al. (2019), peaks around 10 h for solar minimum whereas the duration distribution is broader at solar maximum.

Figure 3 shows the proportion of each plasma origin as a function of $|\sin(\Phi_B - \Phi_P)|$ over the 2008–2018 time range (integrated over all orientations, the proportion of SBO, SRR, CHO, and ejecta categories are 44, 26, 20, and 10%, respectively). For most of the field orientations the proportions remain constant with a majority of SBO plasma, then SRR plasma, then CHO plasma, and finally ejecta which represent about 10% of all solar wind records. This spread between categories was already reported by (Xu and Borovsky, 2015) with similar numbers. It is only close to ortho-Parker orientations that the proportion of SRR and CHO change with an increase of the former and a decrease of the latter. On **Figure 3** this transition is highlighted in the grey box where ortho-Parker orientations ±35° are located. The other two categories remain unchanged. Magnetic field associated with SRR plasma, likely coming from the core of the helmet streamer where magnetic polarity changes, are also likely to have varied orientations and in particular ortho-Parker ones but the decrease in the CHO fraction is less clear.

It should be noted that (Xu and Borovsky, 2015) had also identified that sustained ortho-Parker spiral intervals are mainly of streamer-belt origin (SBO and SRR), "sustained" being defined as intervals of 3 h or more where the IMF longitude stays in the range 70–90° from the Parker spiral direction and the IMF latitude is within 30° of the ecliptic plane.

The distributions of a number of parameters (but not the IMF orientation) depending on the plasma origins have been extensively discussed in Xu and Borovsky (2015) and will not be reproduced here. Let us just discuss the features of M_A which is a key parameter for controlling the magnetosheath dynamics (and magnetosphere response, see Lavraud and Borovsky, 2008; Lavraud et al., 2013) as it will be discussed in the next section. The ejecta and in particular magnetic clouds have notoriously the lowest M_A (the distribution peaking around 5) with the other categories presenting similar distributions. SRR plasmas are more represented for large M_A (i.e., have the largest tail). **Figure 4** does not show the distribution per category (as already shown in Xu and Borovsky, 2015, their Figure 16) but the proportion of each category as a function of M_A. Ejecta are the only category at low M_A. At large M_A the SRR category dominates although it is characterized by low wind velocity; this comes from the fact that the Alfvén velocity is also very low for this type of plasma (with high density and low magnetic field as illustrated on **Figure 2**).

Finally the difference in mean value shown on **Figure 1** is partly due to the fact that SRR plasmas are more represented at ortho-Parker orientations and have anomalously high M_A. Still ortho-Parker orientation of the IMF is largely observed in SBO plasma as this plasma type is dominant (**Figure 3**) and is commonly composed of slow to moderate winds.

The ~20% difference in solar wind mean M_A value for Parker / ortho-Parker orientations of the IMF has a direct influence on the magnetosheath dynamics. In the following we quantify this role by focusing our attention on the triggering of the mirror instability, a ubiquitous process in compressed plasma environments. We shall see how this solves an unanswered question about the prevalence of mirror mode occurrence behind ortho-Parker field orientation.

3 MAGNETOSHEATH PROPERTIES

In this section we explore one physical consequence on the magnetosheath of the large M_A values associated with the ortho-Parker IMF orientation. Here we follow the formalism of (Liu et al., 2007; Génot, 2008) to derive the magnetosheath properties behind a perpendicular shock from the anisotropic set of Rankine-Hugoniot relations. Mirror mode observations are indeed prevalent behind perpendicular shock where they are more clearly identified than in the developed turbulence found downstream of parallels shocks. As noted by Génot (2009) the full anisotropic system of equations cannot be solved completely from upstream conditions because the anisotropy introduces more unknowns than equations. Typically an additional relation with downstream parameters should be considered. Here (like in the papers cited above) we shall choose a typical magnetic field ratio r_s between the downstream magnetosheath field (B_2) and the upstream/IMF (B_1); this ratio is to be found in the range [1,4]. Indices 1/2 are for upstream/downstream regions, respectively. This analytic approach was convincingly compared with observed conditions at the Earth bow shock, at the solar

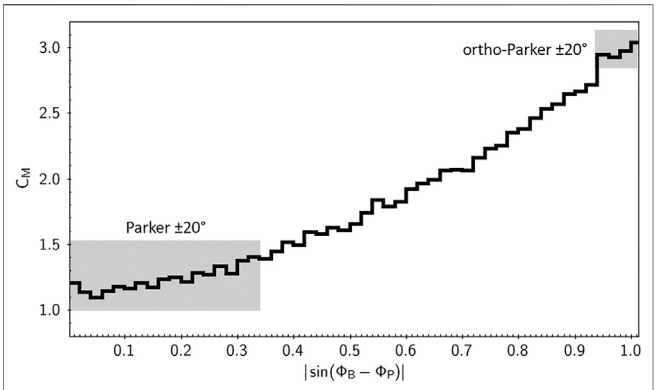

FIGURE 5 | Median of the threshold C_M per bin of $|\sin(\Phi_B - \Phi_P)|$ (for a perpendicular shock with $r_s = B_2/B_1 = 3.5$). Parker orientations ± 20° are shown in the grey box on the left and the ortho-Parker orientations ± 20° are shown in the upper right grey box.

wind termination shock with Voyager data, and with alternative methods (Chao et al., 1995; Liu et al., 2007). For our purpose, this approach allows to express the downstream temperature anisotropy ($A_2 = T_{\perp 2}/T_{\parallel 2}$) and $\beta_{\perp 2}$ as function of the solar wind M_A, β_1, and r_s. For simplicity we chose an isotropic solar wind ($A_1 = 1$).

$$\beta_{\perp 2} = \frac{\beta_1 + 1}{r_s^2} - 1 + \frac{2M_A^2}{r_s^2}\left(1 - \frac{1}{r_s}\right) \tag{6}$$

$$A_2 = \left[\beta_1 + 2M_A^2\left(1 - \frac{1}{r_s}\right) + 1 - r_s^2\right] \times \left[\beta_1(5r_s - 4) + 2M_A^2\left(r_s + \frac{3}{r_s} - 4\right) + 4(r_s - 1)\right]^{-1} \tag{7}$$

Other expressions exist for the parallel shock. For any other shock angle (θ_{Bn}) than 0° and 90° full analytical, however more complex expressions can be used (Génot, 2009). From these downstream parameters the mirror instability criterion C_M can be derived:

$$C_M = \beta_{\perp 2}(A_2 - 1) \tag{8}$$

The magnetosheath plasma is mirror unstable when $C_M > 1$. Note that this common expression for the instability threshold holds in the case of bi-Maxwellian distribution functions and is evaluated in the low-frequency, long-wavelength limit of the Vlasov-Maxwell equations (Stix, 1962; Hall, 1979; Hellinger, 2007). For a chosen compression ratio, or shock strength, (here $r_s = 3.5$ is used) the values of C_M for all solar wind records can be computed. The median value per bin of IMF orientation ($|\sin(\Phi_B - \Phi_P)|$) is shown on **Figure 5**. There is a clear increasing trend from marginal instability threshold ($C_M \simeq 1$) for Parker orientation to more unstable plasma conditions the further the orientation comes closer to ortho-Parker ($C_M \simeq 3$). This shows that, behind a perpendicular shock the magnetosheath plasma is more likely to be mirror-unstable if the orientation of the IMF is ortho-Parker than during the more common Parker orientations. Note that for different shock ratio the behaviour of C_M is similar (increasing with $|\sin(\Phi_B - \Phi_P)|$), the change being on the minimum and maximum values. Indeed, for fixed solar wind (upstream) parameters, following **Eqs. 6**, **7**, the anisotropy and $\beta_{\perp 2}$ decrease for larger shock ratio (which remains less than 4) such that the entropy ($S = \frac{1}{2}k_B \ln(P_\perp^2 P_\parallel/\rho^5)$) increases across the shock.

This result elucidates the observation, yet unexplained, that mirror mode occurrence is larger in planetary magnetosheaths when the IMF orientation is ortho-Parker. This observations was first reported by Génot et al. (2009) during an analysis of 5 years of Cluster data (see their Figure 9) which showed that mirror mode occurrence in the magnetosheath is ~30% larger behind ortho-Parker orientations than behind more common Parker ones. In fact the same behaviour had already been detected with ISEE data but remained unpublished. Further analysis by Dimmock et al. (2015b) using 6 years of THEMIS data reached the same conclusion with the same numbers, including the ~30% increase in mirror mode occurrence for ortho-Parker orientations; yet the underlying reason was not found.

4 DISCUSSION AND CONCLUSION

We have studied 10 years of OMNI solar wind data and characterized the orientations of the IMF at 1 AU with respect to their origin at the Sun. We showed that IMF ortho-Parker orientation is prone to be associated with large M_A plasmas. The typical Alfvén Mach number evolves from a value around 9.5 for Parker orientation (±20°) to ~11.5 for ortho-Parker orientation (±20°). This is a 20% increase. In order to gain more insight into the origin of this distribution we used the plasma characterization scheme of (Xu and Borovsky, 2015). We showed that the variation of the fraction of the different plasma types is relatively small. More precisely, the proportions of the different plasma types are similar in the Parker or ortho-Parker populations with a slight increase for plasmas originating from sector reversal regions. Let us note here that a similar analysis for the previous solar cycle has shown the same trend. Solar wind plasmas associated with sector reversals have typically higher density and lower magnetic field than other categories. This is illustrated in **Figure 2** for instance, and this naturally leads to higher Mach numbers. Also, because of the field reversals and compression zones that characterize these regions, these are more prone to exhibit ortho-Parker field orientations. This is what is suggested on **Figure 3** by the increase of the SRR fraction at large deviation from the Parker spiral. We appreciate the fact that our analysis based on this scheme does not point towards a single origin for the ortho-Parker population. This is not surprising, as Xu and Borovsky (2015) already noted "The origin of several types of solar wind structures such as magnetic holes, ortho-Parker-spiral intervals, and non-ecliptic magnetic field intervals are not known".

Although the origin is not fully understood, the larger M_A values for the ortho-Parker population has noticeable consequences on the magnetosheath that our analysis helped to uncover. By means of anisotropic Rankine-Hugoniot relations we demonstrated that the mirror instability is more likely to be

triggered downstream of perpendicular shocks exposed to ortho-Parker IMF orientation. This was already observed by several *in-situ* missions (ISEE, Cluster, Themis) and partly reported in the literature but no explanation was yet provided.

As noted by Xu and Borovsky (2015) variations with the solar cycle of the fractions of the different categories exist (typically ejecta being more numerous at solar maximum) but the SRR/SBO remain the major ones, which does not affect the main findings of our paper. Our analysis shows that the precise characterization of the ortho-Parker population is not complete. However, two features stand out: the relative fraction of solar wind types change for ortho-Parker orientations in comparison with other orientations, and this population shows larger average M_A with the consequence on the magnetosheath that was exposed in **Section 3**.

Finally, we note that there exist other solar wind categorization schemes which could provide alternative identification of the solar origin of ortho-Parker orientations. However, they cannot be applied on long-term datasets like OMNI. For instance the scheme of Stansby et al. (2019) (used on Helios dataset) requires the temperature anisotropy to separate coronal hole wind (anisotropic) and inter-stream wind (isotropic); see also Neugebauer et al. (2016) for a review of these schemes (as well as Camporeale et al., 2017). As an indication of the high level of intricacy of the solar wind regime characterization, recent results (D'Amicis et al., 2019; D'Amicis et al., 2021) showed that the slow Alfvénic solar wind shares many characteristics of the fast wind (including low compressibility and high correlation between velocity and magnetic field vectors). This is partly studied with the Solar Orbiter and PSP missions at different heliocentric distances.

DATA AVAILABILITY STATEMENT

The raw data supporting the conclusions of this article will be made available by the authors, without undue reservation.

AUTHOR CONTRIBUTIONS

VG and BL did the original data analysis including the figures.

FUNDING

The online analysis tool and database AMDA (http://amda.cdpp.eu/) was used to prepare new datasets from the OMNI original dataset (plasma categorization scheme and magnetosheath properties). AMDA (Jacquey et al., 2010; Génot et al., 2010; Génot et al., 2021) is provided by the Centre de Données de la Physique des Plasmas (CDPP, http://www.cdpp.eu/) supported by CNRS, CNES, Observatoire de Paris, and Université Paul Sabatier, Toulouse, France.

ACKNOWLEDGMENTS

We acknowledge use of NASA/GSFC's Space Physics Data Facility's CDAWeb service and OMNI data (King and Papitashvili, 2005). The data analysis and visualization were done with AMDA and the Topcat tool (Taylor, 2005).

REFERENCES

Borovsky, J. E. (2010). On the Variations of the Solar Wind Magnetic Field about the parker Spiral Direction. *J. Geophys. Res.* 115 (A9), A09101. doi:10.1029/2009JA015040

Bruno, R., and Bavassano, B. (1997). On the Winding of the Imf Spiral for Slow and Fast Wind within the Inner Heliosphere. *Geophys. Res. Lett.* 24 (18), 2267–2270. doi:10.1029/97GL02183

Camporeale, E., Carè, A., and Borovsky, J. E. (2017). Classification of Solar Wind with Machine Learning. *J. Geophys. Res. Space Phys.* 122 (11), 10,910–10,920. doi:10.1002/2017JA024383

Chao, J. K., Zhang, X. X., and Song, P. (1995). Derivation of Temperature Anisotropy from Shock Jump Relations: Theory and Observations. *Geophys. Res. Lett.* 22 (17), 2409–2412. doi:10.1029/95GL02187

D'Amicis, R., Bruno, R., Panasenco, O., and Telloni, D. (2021). First Solar Orbiter Observation of the Alfvénic Slow Wind at 0.64 AU. *Astron. Astrophys.* (in press).

D'Amicis, R., Matteini, L., and Bruno, R. (2019). On Slow Solar Wind with High Alfvénicity: from Composition and Microphysics to Spectral Properties. *Monthly Notices R. Astron. Soc.* 483 (4), 4665–4677. doi:10.1093/mnras/sty3329

Dimmock, A. P., Nykyri, K., Karimabadi, H., Osmane, A., and Pulkkinen, T. I. (2015a). A Statistical Study into the Spatial Distribution and Dawn-Dusk Asymmetry of Dayside Magnetosheath Ion Temperatures as a Function of Upstream Solar Wind Conditions. *J. Geophys. Res. Space Phys.* 120 (4), 2767–2782. doi:10.1002/2014JA020734

Dimmock, A. P., Osmane, A., Pulkkinen, T. I., and Nykyri, K. (2015b). A Statistical Study of the Dawn-dusk Asymmetry of Ion Temperature Anisotropy and Mirror Mode Occurrence in the Terrestrial Dayside Magnetosheath Using THEMIS Data. *J. Geophys. Res. Space Phys.* 120 (7), 5489–5503. doi:10.1002/2015JA021192

Génot, V. (2009). Analytical Solutions for Anisotropic Mhd Shocks. *Astrophys. Space Sci. Trans.* 5 (1), 31–34. doi:10.5194/astra-5-31-2009

Génot, V., Budnik, E., Jacquey, C., Bouchemit, M., Renard, B., Dufourg, N., et al. (2021). Automated Multi-Dataset Analysis (AMDA): An On-Line Database and Analysis Tool for Heliospheric and Planetary Plasma Data. *Planet. Space Sci.* 201, 105214. doi:10.1016/j.pss.2021.105214

Génot, V., Budnik, E., Jacquey, C., Dandouras, I., and Lucek, E. (2009). "Mirror Modes Observed with Cluster in the Earth's Magnetosheath: Statistical Study and Imf/solar Wind Dependence," in *Advances in Geosciences*, 14 (World Scientific), 263–283. doi:10.1142/9789812836205_0019

Génot, V., Jacquey, C., Bouchemit, M., Gangloff, M., Fedorov, A., Lavraud, B., et al. (2010). Space Weather Applications with CDPP/AMDA. *Adv. Space Res.* 45 (9), 1145–1155. doi:10.1016/j.asr.2009.11.010

Génot, V. (2008). Mirror and Firehose Instabilities in the Heliosheath. *Astrophys. J.* 687 (2), L119–L122. doi:10.1086/593325

Hall, A. N. (1979). Finite ion Larmor radius modifications to the firehose and mirror instabilities. *J. Plasma Phys.* 21 (3), 431–443. doi:10.1017/S0022377800022005

Hellinger, P. (2007). Comment on the linear mirror instability near the threshold. *Phys. Plasmas* 14 (8), 082105. doi:10.1063/1.2768318

Jacquey, C., Génot, V., Budnik, E., Hitier, R., Bouchemit, M., Gangloff, M., et al. (2010). AMDA, Automated Multi-Dataset Analysis: A Web-Based Service provided by the CDPP. *Astrophys. Space Sci. Proc.* 11, 239–247. doi:10.1007/978-90-481-3499-1_16

King, J. H., and Papitashvili, N. E. (2005). Solar Wind Spatial Scales in and Comparisons of Hourly Wind and Ace Plasma and Magnetic Field Data. *J. Geophys. Res.* 110 (A2), A02104. doi:10.1029/2004JA010649

Lavraud, B., and Borovsky, J. E. (2008). Altered Solar Wind-Magnetosphere Interaction at Low Mach Numbers: Coronal Mass Ejections: Magnetosphere at Low Mach Numbers. *J. Geophys. Res. Space Phys.* 113 (A9). doi:10.1029/2008JA013192

Lavraud, B., Larroque, E., Budnik, E., Génot, V., Borovsky, J. E., Dunlop, M. W., et al. (2013). Asymmetry of Magnetosheath Flows and Magnetopause Shape during Low Alfvén Mach Number Solar Wind. *J. Geophys. Res. Space Phys.* 118 (3), 1089–1100. doi:10.1002/jgra.50145

Li, B., Cairns, I. H., Gosling, J. T., Steward, G., Francis, M., Neudegg, D., et al. (2016). Mapping Magnetic Field Lines between the Sun and Earth. *J. Geophys. Res. Space Phys.* 121 (2), 925–948. doi:10.1002/2015JA021853

Liu, Y., Richardson, J. D., Belcher, J. W., and Kasper, J. C. (2007). Temperature Anisotropy in a Shocked Plasma: Mirror-Mode Instabilities in the Heliosheath. *Astrophys. J.* 659 (1), L65–L68. doi:10.1086/516568

Lockwood, M., Owens, M. J., and Macneil, A. (2019). On the Origin of Ortho-Gardenhose Heliospheric Flux. *Solar Phys.* 294 (6), 85. doi:10.1007/s11207-019-1478-7

Neugebauer, M., Reisenfeld, D., and Richardson, I. G. (2016). Comparison of Algorithms for Determination of Solar Wind Regimes. *J. Geophys. Res. Space Phys.* 121 (9), 8215–8227. doi:10.1002/2016JA023142

Parker, E. N. (1963). *Interplanetary Dynamical Processes*. New York: Interscience Publishers.

Smith, C. W., and Bieber, J. W. (1991). Solar Cycle Variation of the Interplanetary Magnetic Field Spiral. *Astrophys. J.* 370, 435. doi:10.1086/169830

Stansby, D., Horbury, T. S., and Matteini, L. (2019). Diagnosing Solar Wind Origins Using *In Situ* Measurements in the Inner Heliosphere. *Monthly Notices R. Astron. Soc.* 482 (2), 1706–1714. doi:10.1093/mnras/sty2814

Stix, T. H. (1962). *The Theory of Plasma Waves*. New York: McGraw-Hill.

Taylor, M. B. (2005). "TOPCAT & STIL: Starlink Table/VOTable Processing Software," in *Astronomical Data Analysis Software and Systems Xiv*. Editors P. Shopbell, M. Britton, and R. Ebert (San Francisco: Astronomical Society of the Pacific), 347, 29.

Xu, F., and Borovsky, J. E. (2015). A New Four-Plasma Categorization Scheme for the Solar Wind: 4-plasma Solar-Wind Categorization. *J. Geophys. Res. Space Phys.* 120 (1), 70–100. doi:10.1002/2014JA020412

Conflict of Interest: The authors declare that the research was conducted in the absence of any commercial or financial relationships that could be construed as a potential conflict of interest.

Publisher's Note: All claims expressed in this article are solely those of the authors and do not necessarily represent those of their affiliated organizations, or those of the publisher, the editors and the reviewers. Any product that may be evaluated in this article, or claim that may be made by its manufacturer, is not guaranteed or endorsed by the publisher.